Near-Field Scanning Optical Microscopy (NSOM) Studies of the Relationship between Interchain Interactions, Morphology, Photodamage, and Energy Transport in Conjugated Polymer Films

Thuc-Quyen Nguyen and Benjamin J. Schwartz*

Department of Chemistry and Biochemistry, University of California, Los Angeles, Los Angeles, California 90095-1569

Richard D. Schaller, Justin C. Johnson, Lynn F. Lee, Louis H. Haber, and Richard J. Saykally*

Department of Chemistry, University of California at Berkeley, Berkeley, California 94720

Received: December 11, 2000; In Final Form: March 28, 2001

It is becoming increasingly clear that the way in which a conjugated polymer film is cast affects the interactions between polymer chains and thus the optical and electrical properties of the film. Given that conjugated polymer films cast in different ways also show different nanometer-scale surface topographies, the question that arises is: What is the correlation between surface topography, local chain packing, and the local electronic properties of a conjugated polymer film? In this paper, we address this question using fluorescence near-field scanning optical microscopy (NSOM) to examine films of poly(2-methoxy-5-(2′-ethylhexyloxy)-1,4-phenylene vinylene) (MEH-PPV) that were prepared in different ways. The spatially resolved photoluminescence (SRPL) spectra collected on top of the nanometer-scale topographic features ("bumps") exhibited by spin-cast MEH-PPV films show an enhancement of the red portion of the emission relative to spectra collected from flat regions of the film. Moreover, photooxidative damage (signified by a red-shift and drop in quantum yield of the SRPL) occurs much more quickly in the flat regions of the MEH-PPV films than on the topographic bumps. Taken together, these observations suggest that the bumps on the films correspond to regions in which the chains are packed more tightly: the red-shifted emission results from increased interchain interactions, while the decreased photooxidation rate results from the fact that oxygen cannot easily diffuse between the tightly packed polymer chains. We also find that the spatial homogeneity of MEH-PPV films can be greatly improved by annealing: heating the films above the glass transition temperature removes the topographic features and produces a uniform but weak and red-shifted SRPL due to increased interchain interactions. In contrast to spin-cast films, the SRPL of annealed films undergoes a blue-shift upon photooxidation. This result can be explained by considering the differences between the local chain packing in annealed and nonannealed films, combined with the fact that excitations in the film tend to migrate to low-energy aggregated-chain "traps". All of these results provide insight into how polymer film morphology can be controlled through film processing conditions to improve the optical properties and the performance of electroluminescent devices based on this class of materials.

I. Introduction

Conjugated polymers have been studied extensively for the last several years due to their potential for application in optoelectronic devices such as light-emitting diodes (LEDs),[1,2] photodiodes,[3] photovoltaics,[4] and displays.[5] It is becoming increasingly clear that the performance of devices based on conjugated polymers is strongly affected by the film morphology.[6−8] The reason that film properties are so sensitive to morphology is that when the π-electrons of two conjugated polymer segments are in contact, there can be significant electronic interactions between them. The electronic interactions between two polymer chains are often referred to in the literature as excimers,[9−12] polaron pairs,[13,14] or aggregates.[6,15−23] The subtle distinction between these various interchain entities is that "excimer" denotes a neutral excited state shared between multiple chain segments, while "polaron pair" suggests an excited state characterized by a separation of charge between the chains. "Aggregates" have a ground state that is delocalized between multiple chain segments as well as a delocalized excited state. Given that there are an infinite number of ways the chains can pack in a conjugated polymer film, the interchain species formed are likely to have some of the characteristics suggested by each of these labels: one expects that there is a continuum of delocalized excited states with partial charge-transfer character and that the extent of delocalization can vary between the ground and excited states.

The presence of interchain species in conjugated polymer films has been highly controversial[14,24] largely because the nature of the electronic interactions is extraordinarily sensitive to the distance and relative orientation between the interacting polymer segments.[25] We recently studied films of poly(2-methoxy-5-(2′-ethylhexyloxy)-1,4-phenylene vinylene), MEH-

* To whom correspondence should be addressed. E-mail: schwartz@chem.ucla.edu and saykally@uclink4.berkeley.edu.

10.1021/jp004456e CCC: $20.00
Published on Web 05/11/2001

PPV (see the inset to Figure 2b, below, for chemical structure), and showed that the degree of interchain interactions strongly depends on the polymer film morphology.[6,7] The morphology of spin-cast polymer films can be altered by changing the solvent or the polymer concentration of the solution from which the film is cast[6] or by changing the spin speed.[26] The film morphology also can be modified by annealing the polymer film,[6,7] heating or aging the polymer solution before casting the film,[27] preparing the films layer-by-layer using Langmuir−Blodgett[8] or self-assembly techniques[28] or by changing the nature of the side groups attached to the conjugated polymer backbone.[29] The presence of interchain interactions has important implications for conjugated polymer-based LEDs. Increased interchain interactions promote charge transport but also lower the luminescence quantum efficiency,[6,7] leading to a fundamental tradeoff when trying to optimize film morphology for device performance. With all of this variability in the properties of conjugated polymer films based on processing conditions, it is no wonder that there have been so many conflicting ideas presented in the literature.[14,24] This is because different research groups have their own preferred polymers and methods for film processing, so that the samples in different studies have vastly different degrees of interchain interactions.[6]

The most direct evidence that chain packing and polymer film morphology vary with processing conditions comes from scanning force microscopy (SFM). For MEH-PPV, SFM experiments indicate that spin-cast films are predominantly flat, except for the presence of some roughly circular topographic features that are a few tens of nanometers high and a few hundred nanometers across.[6] The size and number of these topographic bumps correlate with the choice of solvent and concentration of the solution from which the films are cast. In particular, MEH-PPV films cast from "good" solvents,[30] such as chlorobenzene (CB), show an increased number of these topographic features, while MEH-PPV films cast from "poor" solvents,[30] such as tetrahydrofuran (THF), show fewer such features. The number and size of these topographic features increases with increasing polymer concentration in the solution from which the films are cast. There is a direct correlation between films that have large numbers of topographic features and those that show the electronic signatures of high degrees of interchain interaction, including: decreased photoluminescence quantum yield; the presence of a weak, red-shifted feature in the absorption spectrum, excitation of which produces a weak, red-shifted emission that is much longer-lived than the single-chain PL; and enhancement of the rate of exciton−exciton annihilation at high excitation intensities.[6] We have used the label "aggregate" to describe the interchain interactions in MEH-PPV because the presence of the red-shifted absorption band implies a delocalized ground state,[15] although we expect that there is in fact a continuum of different interchain species present in the films.[31] All this work has provided a good understanding of the relationship between polymer morphology and optical properties to devise ways of controlling morphology to enhance the performance of devices based on conjugated polymer films.[7]

The fact that the optical, electrical, and topographic properties of films correlate with the processing conditions indicates that memory of the chain conformation and degree of aggregation of the polymer in solution survives the casting process.[6,15] This suggests that the topographic features seen in the SFM experiments are the result of clumps of entangled polymer chains in the solution that do not break up during spin-coating: the features mark places where the tops of these clumps extend above the average thickness of the film. The bumps on the surface of the film would then correspond to regions of highly aggregated polymer chains. Thus, the correlation between the number and size of the SFM bumps with the electronic properties of the bulk films makes sense because we can associate the presence of bumps on the films with the electronic signatures of interchain interactions.[6] This overall picture of polymer solution properties controlling film morphology, and hence device behavior, hangs together quite nicely, but up to this point we have no direct proof that the topographic features seen by SFM are in fact associated with increased interchain interactions. The optical and device measurements that indicated aggregation in our previous work were performed over large film areas, so all the results were a spatial average of behaviors associated with both the bumps and the flat regions of the films.[6,7]

In addition to aggregation and interchain interactions, oxidative damage is another critical factor in determining the luminescence efficiency of conjugated polymer devices. It is well documented that conjugated polymers can easily photooxidize, producing carbonyl groups that break the conjugated backbone.[32] These carbonyl defects decrease the average conjugation length and also act as efficient traps that quench the luminescence.[33] In our previous work, we noticed that the rate at which MEH-PPV films undergo photooxidation is strongly morphology dependent: photoinduced damage is slower in MEH-PPV films cast from CB, which have higher degrees of interchain interactions (as well as more of the topographic bumps seen by SFM), and faster in MEH-PPV films cast from THF.[6] The picture that explains this result is that films with high degrees of interchain interactions have their chains packed tightly enough that oxygen cannot easily penetrate into the film, lowering the rate at which photooxidation can occur. Films with a lower degree of interchain interactions, on the other hand, have an increased frequency of voids between the more loosely packed chains that allow oxygen to diffuse easily to photoexcited regions in the interior of the film, leading to more rapid oxidative damage. Thus, the way the chains pack in conjugated polymer films not only affects the presence of interchain electronic species but also determines how susceptible the films are to photooxidation.

In this paper, we describe a collaborative effort between our groups at UCLA and Berkeley to examine the effects of local chain packing on both the polymer electronic structure and the susceptibility to damage by taking advantage of near-field scanning optical microscopy (NSOM). NSOM has been proved an effective technique for studying the optical properties of organic materials and biological systems on nanometer length scales.[34] In NSOM, a tapered optical fiber with a sub-wavelength-sized aperture is scanned over the sample with the tip held close to the surface in the near-field regime. The feedback electronics used to hold the sample-tip distance constant provide for simultaneous measurement of the surface topography and the optical properties of a sample. The technique provides spatial resolution that is determined by the tip diameter, which easily can be made ∼75−150 nm, surpassing the far-field diffraction limit ($\sim\lambda/2$). This means that NSOM provides a spatial resolution that is ideal for probing the optical properties of the topographic features seen on the surface of MEH-PPV films. Thus, using NSOM, we can investigate how the electronic properties of MEH-PPV vary spatially in the film and how they correlate with the film morphology.

Blatchford et al. previously have used NSOM to study films of poly(*p*-pyridyl vinylene), PPyV, and found evidence of aggregated domains with a size on the order of 200 nm.[21] These

workers did not find any correlation between the film topography and the intensity or polarization of the photoluminescence (PL). A similar set of experiments performed by Buratto and co-workers on films of (unsubstituted) PPV found aggregated domains ~100 nm in diameter in which there was a correlation between the film topography, the PL intensity, and the emission polarization.[35] While none of this previous work investigated the spectrum of the spatially resolved photoluminescence (SRPL), the measurements from both groups do show that aggregated species may exhibit spatial localization, indicating that the optical properties of a conjugated polymer sample can vary from location to location within the film. NSOM has also been used to study films of liquid crystalline poly(9,9-dialkylfluorenes),[29] which reveal two distinct types of morphology: 50−150 nm polymer clusters that have a lower PL quantum yield than the rest of the film, and 50−500 nm polymer domains that show highly polarized luminescence. There is a direct correlation between the low-PL-quantum-yield clusters and the topography, but no correlation was found between the polarized PL domains and the topography.[29] From all of these studies, the logical questions that remain are (1) How do the differences in the local environment affect the performance of devices based on conjugated polymer films? (2) Given the relationship between film morphology and interchain interactions, how can the local environments of a conjugated polymer film be manipulated or controlled to optimize the properties for desired device applications?

In this collaborative work, we will address these questions by using NSOM to show that there is a direct correlation between the nanometer-scale topography/morphology of a conjugated polymer film and the local electronic properties. We will concentrate our efforts on MEH-PPV films, so that we can make direct ties to our previous work studying the interchain interactions in MEH-PPV films cast from CB and THF and in MEH-PPV films that have been annealed.[6] Unlike the NSOM work described above in which the polymer was excited through the NSOM tip and the emission was collected in the far-field ("illumination mode"),[21,29] in the present experiments the MEH-PPV films are excited in the far-field and the PL is collected through the tip. Using this "collection mode" geometry, which allows us to measure SRPL spectra with an invariant tip/field geometry,[36] we find that both the spectrum of the SRPL and the rate of photooxidative damage varies significantly from location to location within the same film. Moreover, both the SRPL spectrum and the damage rate correlate directly with the surface topography. Since the surface topography correlates with the film casting conditions, the results help us to complete our picture of the relationship between processing conditions, morphology, and interchain interactions in conjugated polymer films on the nanometer scale. In addition to learning about interchain interactions and chain packing, our investigations also help to characterize the energy transfer in conjugated polymer films. By comparing the damage rates of the single-chain and aggregated PL, we show that energy transfer moves excitations toward aggregated sites. Thus, the presence of an aggregated "defect" can quench fluorescence from many nearby chromophores via energy transfer. Taken together, all of the results provide useful information for optimizing interchain interactions to produce improved polymer-based LEDs.

II. Experimental Methods

MEH-PPV was synthesized according to methods described previously in the literature.[37] All the polymer solutions and films were prepared in an inert N_2 atmosphere. MEH-PPV was dissolved in THF and CB in the dark for several hours to give 1% (w/v) solutions. The polymer solutions were spin-cast onto cleaned glass substrates, and the resulting films were heated at 50 °C for several hours to evaporate any residual solvent. To produce annealed films, the films were heated above the polymer glass transition temperature (~205 °C for our polymer with molecular weight $\sim 1 \times 10^6$)[6] for several hours under a nitrogen atmosphere.

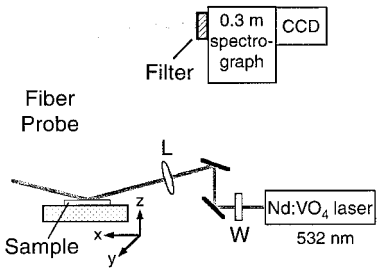

Figure 1. Near-field scanning optical microscopy (NSOM) experimental setup.

The Berkeley NSOM system,[36] equipped with a nonoptical, noncontact (~5−10 nm separation) shear-force feedback mechanism and closed-loop piezo scanner was employed for near-field SRPL measurements of the MEH-PPV films. Chemically etched SiO_2 fiber optic probes with a ~75 nm diameter aperture (as measured via SEM) were produced following the procedure described in reference;[38] metal coatings were not used on the tips to avoid perturbing the observed spectra via the Stark effect. All topographical images were scanned over a 10×10 μm area and consist of a 200×200 pixel array. The lateral resolution is estimated to be ~160 nm;[36] the black-to-white color scale in the topographic images presented below correspond to a height difference of ~50 nm. To control the atmosphere around the sample during excitation, the entire NSOM system was sealed in a box, which could be purged with dry nitrogen gas. As shown in Figure 1, near-field measurements were conducted in an oblique collection mode geometry with the optical excitation incident upon the sample 60° from normal incidence. Collection mode provides the advantage of higher spatial resolution than illumination mode when using uncoated tips because the luminescence field intensity decays exponentially from the surface, so that a small amount of leakage is not detrimental to the resolution. A leaky tip in illumination mode, in contrast, provides a significantly decreased resolution because the emission from regions excited out of the near-field are still collected by the far-field optics. The excitation light had horizontal polarization at the position where the fiber probe collected emission from the sample. To maintain a constant tip/field geometry, the NSOM probe and excitation laser spot remained static during all measurements; spatial motion was performed by scanning the sample stage in the *x* and *y* as well as the *z* (feedback) directions. After measuring the topography of a region, the near-field probe was directed via computer control to different positions of the sample (always maintaining near-field feedback), and SRPL spectra were acquired at each indicated point.

SRPL measurements were performed using a diode-pumped, frequency-doubled Nd:VO_4 laser (Spectra-Physics) (~50 μW, 532 nm, CW) as the excitation source. The laser beam was focused with an 8-cm focal length lens to produce a ~200 μm diameter spot on the sample. Optical signals were collected by the near-field probe and directed via the fiber optic through a 532-nm holographic notch filter and a 1/3-m spectrograph. After dispersing the PL signal with a 150-gr/mm grating, the spectrally

resolved PL was detected with a nitrogen-cooled, back-illuminated CCD camera. All of these measurements were conducted under a nitrogen atmosphere. At this low excitation intensity, photodamage to the sample was not observed, and the acquired SRPL spectra for a given area were completely reproducible as a function of time. All the displayed SRPL spectra are the sum of five accumulations of individual scans integrated for 5 s. For all the data presented below, hundreds of spectra were acquired for multiple regions on each of multiple MEH-PPV films cast from each solvent. For the as-cast films discussed below, the main variation in the SRPL spectra collected from different locations or different samples was a variation in the relative heights of the two main emission peaks at 570 and 620 nm; the positions and number of the bands in the spectrum did not change from region to region or film to film. The spectra selected for the figures below were chosen to be representative of the majority of the sampled regions; they are by no means the most dramatic examples of spectral variation that we observed in the course of this study.

Photodamage experiments were conducted in a manner similar to SRPL measurements. For each measurement, after the sample topography was acquired, the sample was continuously excited with 3 mW of 532-nm light (60× SRPL intensity) for 15 min; spectra were recorded every 10 s with the CCD during this time. A different region of the sample was used for each photodamage measurement by moving the sample perpendicularly to the excitation plane to avoid regions of the sample that may have been exposed to reflections of the excitation light. Experiments were first conducted under a nitrogen atmosphere and subsequently studied under ambient conditions to investigate the effect of oxygen on the photodamage rate.

III. Results and Discussion

Even though it is becoming clear that processing conditions affect the morphology of conjugated polymer films, which in turn changes the physics of devices based on these materials, the questions remain: how does the local variation in morphology of a film influence the local electronic properties and hence the bulk photophysics of the film? How can these local structures be controlled or manipulated? To answer to these questions, we take advantage of the NSOM technique, which allows us to probe the optical properties of different local structures within the same conjugated polymer film. Information from these experiments is important to improve the performance of the polymer-based devices.

A. Correlation Between Interchain Species and Film Topography. Topographical images and SRPL spectra of MEH-PPV films prepared with different processing conditions are shown in Figure 2. For each processing condition, we performed measurements on many regions of each of multiple films, and we found qualitatively similar results for each type of film. Thus, in the data presented below, only representative scans for each type of film are shown.

Figure 2a (right) shows the topography of an MEH-PPV film cast from CB over a $(5\ \mu m)^2$ region. In agreement with our previous work using SFM,[6] the topography is predominantly flat with small features that are a few hundred nanometers in diameter and ~10 nm high. The left-hand plot in Figure 2a shows the SRPL spectra obtained with the sample excited in the far field at two different positions on the film. As shown on the topographic profile, position 1 is on the top of one of the bumps and position 2 is centered in one of the flat regions of the film. Even though the two SRPL spectra are collected

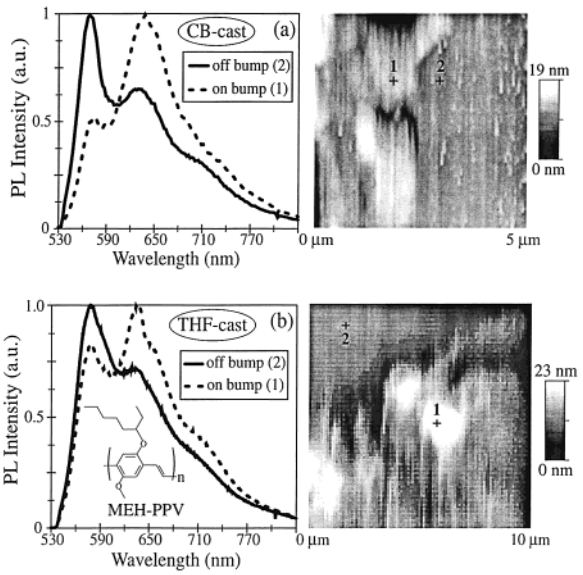

Figure 2. Topographic profiles (right) and normalized spatially resolved photoluminescence (SRPL) spectra (left) of MEH-PPV films in different environments cast from 1% w/v solutions. (a) Topography over a 5 × 5 μm area of an MEH-PPV film cast from CB (left) and SRPL (right) collected on one of the bumps (dashed curve) and from a flat region of the film (solid curve). (b) Topography over a 10 × 10 μm area of an MEH-PPV cast from THF (right) and SRPL (left) collected on one of the bumps (dashed curve) and from a flat region of the film (solid curve). The inset shows the chemical structure of MEH-PPV.

only ~1 μm apart, they are clearly different, showing that the emission from MEH-PPV films, like that of other conjugated polymers,[21,29,35,39] is spatially inhomogeneous. The SRPL spectrum collected from the flat region (position 2, solid curve) strongly resembles that of MEH-PPV in solution, while the spectrum collected on top of the bump (position 1, dashed curve) shows a red tail and a relative enhancement of the vibronic feature near 620 nm. This relative enhancement of the red portion of the emission, which we observe when collecting SRPL from most of the topographic features (and only occasionally from the flat film regions), is a direct signature of interchain interactions. The weak red PL tail is the emission from aggregated chromophores,[6,12] while the relative PL enhancement near 620 nm results from a change in vibronic coupling characteristic of MEH-PPV chromophores in regions with tightly packed chains.[6,40] The fact that the characteristic interchain emission correlates with the topographic features supports our assignment of the features to aggregated clumps of polymer chains that survive the casting process from solution. The occasional presence of the signature interchain emission in the flat regions of the film likely corresponds to aggregated polymer clumps that happen to reside near (but do not extend above) the film's surface. The presence of the more characteristic single-chain emission from some of the topographic features indicates that simply tangling the chains in solution does not ensure that the polymer chromophores will interact with each other. Moreover, as we will discuss further below, it is also possible that there is not a good pathway for energy to transfer from single chains to the aggregated chromophores in every bump, so that some bumps still show the characteristic single-chain emission. Despite these occasional exceptions, the overall correlation remains strong: the topographic features are associated with regions of greater degrees of interchain interactions.

Figure 2b shows the topography of MEH-PPV films cast from THF (right) and the SRPL spectra (left) collected on the top of

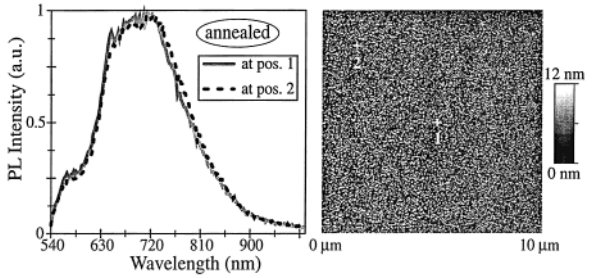

Figure 3. The topography over a 10 × 10 μm area (right) of an annealed MEH-PPV film and normalized SRPL spectra (left) collected at two different positions on the film.

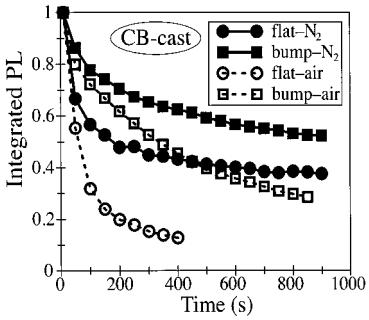

Figure 4. The integrated SRPL intensity of an MEH-PPV film cast from CB in nitrogen (solid symbols) and in the presence of ambient oxygen (open symbols) collected on the top of a bump (circles) and from a flat region of the film (squares).

a bump (dashed curve, position 1) and on a flat region (solid curve, position 2). In agreement with our previous work using SFM, the THF-cast films also show occasional topographic bumps but at a much lower density than seen in the CB-cast films studied in Figure 2a. Also unlike the CB-cast films, there is little difference in the SRPL spectra collected on and off the bumps, although on average there is a slight increase in the intensity of the red emission tail and the 620-nm vibronic feature when collecting on the bumps. This suggests that there is little local chromophore aggregation in MEH-PPV films cast from THF, in agreement with the conclusions of our earlier work on bulk films.[6] The presence of topographic features in these THF-cast films emphasizes an important distinction between physical aggregation of the polymer chains and photophysical aggregation of the conjugated chromophores. The polymer chains definitely clump together in "poor" solvents[30] like THF, leading to topographic bumps in the films whose size increases with increasing polymer concentration in the solution from which the film is cast.[6] The tightly coiled chains in THF solution, however, do not provide access for chromophores (which typically extend over 4−6 repeat units of the polymer) to strongly interact with each other.[15] Thus, Figure 2b shows that although the MEH-PPV chains in films cast from THF can be aggregated, there is comparatively little chromophore aggregation, leading to fewer signs of interchain electronic species.

Figure 3 shows the topography (right) and SRPL spectra (left) of an annealed MEH-PPV film. In our previous work, we found that heating conjugated polymer films above T_g allowed the chains to flow, so that annealed films have a much flatter surface topography seen with SFM than as-cast films.[6] Upon cooling, the flowing chains tend to pack into low energy structures with a high degree of interchain interaction. This leads to annealed films whose emission is almost entirely quenched: the little fluorescence that remains peaks near 700 nm, the result of the very weak emission from aggregated chromophores.[6,12] The NSOM results in Figure 3 make it clear that the annealed films have a spatially uniform structure, both topographically and electronically: the MEH-PPV chromophores have a high degree of interaction throughout the film. The NSOM experiments also show that once annealed, the film has no memory of its initial morphology: both CB and THF-cast annealed films show identical topographical and optical behavior. Thus, Figure 3 shows only the data for a THF-cast annealed MEH-PPV film; the data for annealed films cast from any solution are qualitatively similar. The interchain emission that dominates the PL from annealed MEH-PPV films is so weak because it has an extraordinarily long radiative lifetime, so that nonradiative processes can significantly reduce the emission quantum yield.[10,12] This explains why the presence of interchain species in conjugated polymer films is so detrimental to luminescence efficiency: excitations on aggregated chromophores, whether directly excited or populated by energy transfer, have a high probability for nonradiative deactivation.

B. Correlation between Photooxidative Damage and Film Topography. In addition to interchain interactions, it is well-known that photooxidation of conjugated polymer films can lead to quenching of the PL,[32,33] even at relatively low excitation intensities.[6,41] The photophysical signatures of photodegradation include: a blue-shift and decrease in the intensity of the ground-state absorption band;[42] the presence of a photoinduced absorption (PA) in the emission region in pump−probe experiments;[6,41,43] and a reduced PL quantum yield.[6,32,33] To investigate the dynamics of photodegradation, we exposed MEH-PPV films to higher excitation laser intensities and collected the SRPL as a function of time both in ambient conditions and under a nitrogen atmosphere to examine the effects of oxygen on the photostability.

Figure 4 shows spectrally integrated SRPL intensities from an MEH-PPV film cast from CB, with the SRPL collected both on top of the topographic bumps (squares) and away from the bumps (circles) when the films are excited in air (open symbols) or under the nitrogen purge (solid symbols). In both air and the nitrogen purge, the decay of the SRPL is slower when collecting emission from the top of a bump than when probing away from a bump. Qualitatively similar results are observed for collecting emission on and off the bumps from MEH-PPV films cast from THF. This difference in the integrated SRPL decay provides direct evidence that the polymer chains are packed differently in different spatial regions of the film. The slower photodamage rate on the bumps is easy to rationalize using the information from the last section. If the bumps correspond to regions of highly tangled polymer chains, then it is difficult for O_2 to penetrate below the surface of the film in these regions. Thus, the surface of the film photooxidizes quite rapidly, producing the initial rapid loss of SRPL intensity, but the chromophores below the surface are protected, leading to a relatively stable, long-lived PL. When collecting SRPL from the flat regions where the polymer chains have a more open conformation, O_2 can more easily penetrate below the film's surface, leading to rapid photooxidative damage that causes a continuous drop in the integrated SRPL intensity.

In addition to demonstrating that the local chain packing correlates with the presence of the topographic features, the data in Figure 4 also show that the presence of O_2 is important in the photodamage mechanism. When probing both on and off the bumps, the photodegradation decay dynamics are much faster in ambient oxygen than in a nitrogen atmosphere. This result is not surprising given that we expected photooxidation to be a serious concern for the PL from these materials. In fact, Buratto and co-workers have taken advantage of this type of

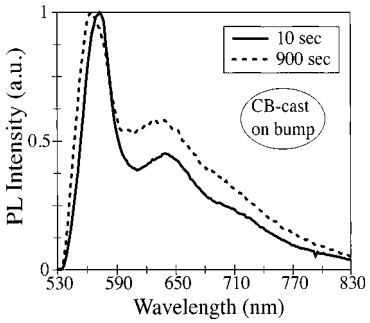

Figure 5. Normalized SRPL spectra of an MEH-PPV film cast from CB collected in the presence of ambient oxygen as a function of time following exposure to the excitation laser: 10 s (solid curve) and 900 s (dashed curve).

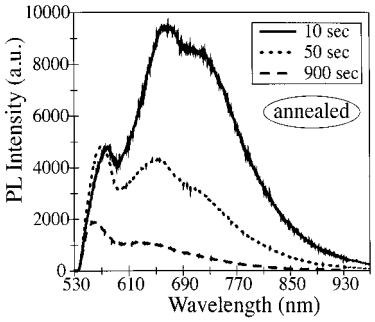

Figure 6. Normalized SRPL spectra of an annealed MEH-PPV film collected in the presence of ambient oxygen as a function of time following exposure to the excitation laser: 10 s (solid curve), 50 s (dotted curve), and 900 s (dashed curve).

photoinduced oxidative damage to use near-field excitation to photopattern conjugated polymer films via spatial hole-burning.[44] The small amount of photodamage that occurs under the nitrogen purge can be explained both by the photoreactivity of intrinsic defects (such as chain ends or oxygen trapped in the polymer bulk) and by the small amount of oxygen that the purge simply does not remove. Overall, the fast SRPL decay component seen in all the traces in Figure 4 most likely results from a combination of intrinsic defects already present in the film and direct photooxidative attack on the surface of the film. The slower SRPL decay component can be assigned to the time it takes for oxygen to diffuse from the air to the photoreactive sites below the film's surface.

C. Energy Transport Unveiled by NSOM Photodamage Studies. One of the most important features of the photophysics of conjugated polymer films is the rapid energy transfer that takes place between conjugated segments. A wide variety of work has established that the correct "zeroth order" picture of a conjugated polymer chain is that of a series of linked chromophores, each with a different conjugation length. In polymer films, excitations move rapidly from the shortest conjugated segments, which are higher in energy, to the longest conjugated segments, which are lower in energy.[45] Experiments examining the flow of energy in isolated MEH-PPV chains encapsulated in the channels of a mesoporous silica glass[46] have determined that intrachain (along the chain backbone) energy migration is 2 orders of magnitude slower than interchain (through space) energy transport via Förster transfer, which takes only a few picoseconds.[47] This rapid interchain energy transport has important consequences for light-emitting devices based on these materials: since excitations can rapidly transfer between polymer chains, they can easily migrate to aggregated sites or other low-energy defects, leading to quenching of the emission.

Figure 5 shows representative SRPL spectra collected from one of the topographic features on a CB-cast film of MEH-PPV in air at two different times following continuous exposure to the excitation laser: 10 s (solid curve) and 900 s (dashed curve). Integrating the spectra in this figure produces two of the open squares in the SRPL decay curve discussed in the last section and presented in Figure 4. To better illustrate how the shape of the spectrum changes with time, the spectra in Figure 5 are normalized to the SRPL maximum, even though the total integrated intensity has decreased by a factor ≥ 3 during the 890-s interval shown. At early times, before much photoinduced degradation has occurred (10 s, solid curve), the SRPL spectrum shows the characteristic signatures of interchain interactions. This suggests that energy from many of the single chromophores is funneled to a few sets of aggregated chromophores, explaining why the extremely weak aggregate emission comprises such a significant fraction of the overall SRPL spectrum. At later times, after the film has undergone significant photooxidative damage (900 s, dashed curve), it is clear that the main peak of the SRPL has moved to the blue and that the red PL tail now comprises a much larger fraction of the overall spectrum. The blue-shift of the main SRPL peak is a direct reflection of the shorter average conjugation length following photooxidation. The relative enhancement of the red tail of the SRPL spectrum shows that the damage has disproportionately affected the single-chain chromophores, so that emission from interchain species now comprises a larger fraction of the SRPL. This result implies that despite the differences in excited-state lifetime, the single-chain chromophores are more susceptible to photooxidation than the aggregated chromophores, consistent with our general picture that the tightly tangled aggregated chains are more impervious to O_2.

Figure 6 shows the results of a similar set of experiments on annealed MEH-PPV films photoexcited in the presence of ambient oxygen, with representative SRPL spectra displayed at a few select times under continuous photoexcitation. Unlike the data in Figure 5, the data in Figure 6 are presented as measured and have not been normalized or scaled in any way. Even without normalizing the spectra, it is clear from Figure 6 that the SRPL of the annealed film undergoes dramatic changes in shape as photodamage occurs. In the annealed film, nearly all the polymer chromophores are in aggregated sites, and there are only occasional single chromophores embedded within the mass of aggregated chains. The excitations on most of these single chromophores rapidly (within a few ps[47]) undergo energy transfer to nearby aggregated sites, leading to a SRPL spectrum dominated by interchain species. This means that excitations in the annealed film spend most of their time on aggregated sites, so these are the sites where photooxidative attack occurs most readily. As a result, photooxidation damages the aggregated sites at the bottom of the energy funnel first, leaving behind the few single-chain chromophores. This shows up in Figure 6 as a relative enhancement of the blue portion of the SRPL spectrum at later times, showing that single-chain emission is becoming more important with respect to the interchain emission that is undergoing photodegradation.

Overall, the data in Figures 5 and 6 illustrate that the way in which photooxidation of conjugated polymer takes place depends on a tradeoff between where the photoexcitations spend most of their time, and how accessible the chromophores are to oxygen, both determined by the local chain packing. In nonannealed films, there are many single-chain chromophores that are not connected by energy transfer pathways to aggregated sites. Thus, many excitations spend most of their time on the single-chain chromophores, and those that are accessible to

oxygen undergo rapid photodamage, leading to a red-shift of the SRPL spectrum as the interchain emission increases in relative importance. In annealed films, the few single chain chromophores that emit before undergoing transfer to an interchain site are highly protected from oxygen by the surrounding aggregated chains. This means that photooxidation affects the interchain sites at the bottom of the energy funnel first, leading to a blue-shift of the SRPL spectrum as the single-chain emission increases in relative importance. These ideas are in agreement with the recent work of Barbara and co-workers[48] as well as Huser et al.,[49] who studied the PL of single MEH-PPV molecules. Depending on how the single MEH-PPV chains were folded, these workers found that photooxidation could produce either a red-shift or a blue-shift of the PL, in direct correlation to whether there was an efficient energy funnel connecting the high-energy and low-energy chromophores. The NSOM results presented here provide a way to examine these photophysical processes in films without having to use far-field collection, which spatially averages over all of the inhomogeneous regions present within the bulk.

IV. Conclusions

In summary, we have demonstrated that there is a direct correlation between the nanoscale topography and the local optical properties of the MEH-PPV films. By spectrally resolving the SRPL, we have observed the spectroscopic signatures of high degrees of interchain interactions in spatial regions correlated with physical bumps. This result is consistent with a picture in which polymer aggregates that are present in solution survive the casting process and persist into the film, so that the solution processing conditions control both the local morphology and electronic properties. We also have found that the rate of spatially resolved photodegradation differs significantly in different regions of an MEH-PPV film: the photodegradation rate is a factor of $\sim$2 slower on the topographic bumps than on the flat regions. The presence of ambient oxygen significantly accelerates the rate at which photodamage occurs, suggesting that the primary damage mechanism is photooxidation of the polymer to produce nonradiative quenching centers. The slower photooxidation rate on the topographic features can be explained by the fact that the polymer chains comprising the bumps are tightly packed, hindering the diffusion of oxygen into these regions of the film. Examination of the spectral shifts of the SRPL also provides insight into energy transport in the films. The fact that as-cast MEH-PPV films show a red-shift of the SRPL spectra upon photodegradation while annealed films show a SRPL blue-shift indicates that both energy transport and local chain packing are important in determining behavior of these complex materials.

All of these results have important implications for the design of devices based on these materials. The spatial inhomogeneity with respect to chain packing and electronic aggregation may be responsible for one of the most important device failure mechanisms: the development of "black spots".[50] Since the topographic bumps on the film's surface have a larger degree of interchain packing, there will be enhanced current injection into these regions, which also have a lower luminescence quantum efficiency because the chromophores are aggregated. As the current runs preferentially through these regions, they may heat up and become annealed, which would further increase the current flow and decrease the luminescence efficiency. As this process continues, an entire region of the film becomes nonemissive, producing a black spot. Eventually, the device fails due to a pinhole short as an annealed pathway develops through the film and bridges the electrodes. Even if it is not directly responsible for the formation of black spots, the spatial inhomogeneity present in conjugated polymer films does not bode well for device efficiency: the carriers have the highest mobility in regions with high degrees of interchain interactions and thus will tend to recombine in these regions. Unfortunately, these are the exact same regions where energy transfer can easily carry excitations to interchain defects that have a poor luminescence quantum yield.

The above analysis argues that one of the best ways to improve the efficiency of a conjugated-polymer device is to develop processing techniques that result in more spatially homogeneous conjugated polymer films. One way to do this is to choose film casting conditions that provide the most spatially homogeneous film. For example, a recent NSOM study by Huser and Yan, which appeared after the original submission of this paper, has shown that MEH-PPV films cast from some solvents may be quite spatially homogeneous.[51] Another, perhaps preferable way to ensure homogeneity is by annealing the film. Even though the luminescence from annealed films is strongly quenched, the improvement in spatial homogeneity leads to increased electroluminescence efficiency for annealed LEDs as compared to LEDs fabricated from as-cast films.[7] Of course, annealing the film also improves injection at the electrode interfaces, so that the improvement in efficiency in annealed LEDs may result from more balanced charge injection.[52] Nevertheless, the implications are clear: processing conditions need to be controlled to reduce the spatial inhomogenity of conjugated polymer films to optimize their electronic properties for optoelectronic applications.

Acknowledgment. The authors thank Steve Buratto for many stimulating discussions regarding all aspects of this work. The UCLA group is supported by the National Science Foundation under grant DMR-9971842, and the Berkeley group by the National Science Foundation under Grant CHE-9727302. B.J.S. is a Cottrell Scholar of Research Corporation and an Alfred P. Sloan Foundation Fellow.

References and Notes

(1) For recent reviews, see Lovinger, A. J.; Rothberg, L. J. *J. Mater. Res.* **1996**, *11*, 1581 and Friend, R. H.; Gymer, R. W.; Holmes, A. B.; Burroughes, J. H.; Marks, R. N.; Taliani, C.; Bradley, D. D. C.; Dos Santos, D. A.; Bredas, J. L.; Logdlund, M.; Salaneck, W. R. *Nature* **1999**, *397*, 121.

(2) Burroughes, J. H.; Bradley, D. D. C.; Brown, A. R.; Marks, R. N.; Mackay, K.; Friend, R. H.; Burn, P. L.; Holmes, A. B. *Nature* **1990**, *347*, 539; Gustafsson, G.; Cao, Y.; Treacy, G. M.; Klavetter, F.; Colaneri, N.; Heeger, A. J. *Nature* **1992**, *357*, 477.

(3) Granstrom, M., Petritsch, K.; Arias A. C.; Lux A.; Andersson M. R.; Friend, R. H. *Nature* **1998**, *395*, 257

(4) Sariciftci, N. S.; Smilowitz, L.; Heeger, A. J.; Wudl, F. *Science* **1992**, *258*, 1474.

(5) See, e.g., Hebner T. R.; Wu, C. C.; Marcy, D.; Lu, M. H.; Strum, J. C. *Appl. Phys. Lett.* **1998**, *72*, 519; Bharathan, J.; Yang, Y. *Appl. Phys. Lett.* **1998**, *72*, 2660.

(6) Nguyen, T.-Q.; Martini, I.; Liu, J.; Schwartz, B. J. *J. Phys. Chem. B* **2000**, *104*, 237.

(7) Nguyen, T.-Q.; Kwong, R. C.; Thompson, M. E.; Schwartz, B. J. *Appl. Phys. Lett.* **2000**, *76*, 2454.

(8) Sluch, M. I.; Pearson, C.; Halim, M.; Samuel, I. D. W. *Synth. Met.* **1998**, *94*, 285.

(9) Samuel, I. D. W.; Rumbles, G.; Collison, C. J. *Phys. Rev. B* **1995**, *52*, R11573.

(10) Samuel, I. D. W.; Rumbles, G.; Collison, C. J.; Friend, R. H.; Moratti, S. C.; Holmes, A. B. *Synth. Met.* **1997**, *84*, 497.

(11) Jenekhe, S. A.; Osaheni, J. A. *Science* **1994**, *265*, 765.

(12) Jakubiak, R.; Collison, C. J.; Wan, W. C.; Rothberg, L. J. *J. Phys. Chem. A.* **1999**, *103*, 2394.

(13) Yan, M.; Rothberg, L. J.; Kwock, E. W.; Miller, T. M. *Phys. Rev. Lett.* **1995**, *75*, 1992.

(14) Yan, M.; Rothberg, L. J.; Papadimitrakopoulos, F.; Galvin, M. E.; Miller, T. M. *Phys. Rev. Lett.* **1994**, *72*, 1104.

(15) Nguyen, T.-Q.; Doan, V.; Schwartz, B. J. *J. Chem. Phys.* **1999**, *110*, 4068.

(16) Lemmer, U.; Heun, S.; Mahrt, R. F.; Scherf, U.; Hopmeier, M.; Siegner, U.; Gobel, E. O.; Mullen, K.; Bassler, H. *Chem. Phys. Lett.* **1995**, *240*, 373.

(17) Pauck, T.; Hennig, R.; Perner, M.; Lemmer, U.; Siegner, U.; Mahrt, R. F.; Scherf, U.; Mullen, K.; Bassler, H. *Chem. Phys. Lett.* **1995**, *244*, 171.

(18) Mahrt, R. F.; Pauck, T.; Lemmer, U.; Sieger, U.; Hopmeier, M.; Hennig, R.; Bassler, H.; Gobel, E. O.; Bolivar, P. H.; Wigmann, G.; Kurz, H.; Scherf, U.; Mullen, K. *Phys. Rev. B* **1996**, *54*, 1759.

(19) Grell, M.; Bradley, D. D. C.; Long, X.; Chamberlain, T.; Inbasekaran, M.; Woo, E. P.; Soliman, M. *Acta Polym.* **1998**, *49*, 439.

(20) Blatchford, J. W.; Jessen, S. W.; Lin, L.-B.; Gustafsson, T. L.; Fu, D.-K.; Wang, H.-L.; Swager, T. M.; MacDiarmid, A. G.; Epstein, A. J. *Phys. Rev. B* **1996**, *54*, 9180.

(21) Blatchford, J. W.; Gustafsson, T. L.; Epstein, A. J.; Vanden Bout, D. A.; Kerimo, J.; Higgins, D. A.; Barbara, P. F.; Fu, D.-K.; Swager, T. M.; MacDiarmid, A. G. *Phys. Rev. B* **1996**, *54*, R3683.

(22) Hsu, J. H.; Fann, W. S.; Tsao, P. H.; Chuang, K. R.;Chen, S.-A. J. *Phys. Chem. A* **1999**, *103*, 2375; Chang, R.; Hsu, J. H.; Fann, W. S.; Yu, J.; Lin, S. H.; Lee, Y. Z.; Chen, S. A. *Chem. Phys. Lett.* **2000**, *317*, 153.

(23) Zheng, M.; Bai, F.; Zhu, D.; *J. Photochem. Photobio. A* **1998**, *116*, 143.

(24) While several groups have argued that the majority of excitations result in interchain species (see, e.g., refs 6, 10, 12, and 13), there also have been reports that the branching ratio for interchain species formation is essentially zero; see, e.g., Greenham, N. C.; Samuel, I. D. W.; Hayes, G. R.; Phillips, R. T.; Kessener, Y. A. R. R.; Moratti, S. C.; Holmes, A. B.; Friend, R. H. *Chem. Phys. Lett.* **1995**, *241*, 89; Frolov, S. V.; Liess, M.; Lane, P. A.; Gellermann, W.; Vardeny, Z. V.; Ozaki, M.; Yoshino, K. *Phys. Rev. Lett.* **1997**, *78*, 4285; Becker, H.; Burns, S. E.; Friend, R. H. *Phys. Rev. B* **1997**, *56*, 1893.

(25) Cornil, J.; Dos Santos, D. A.; Crispin, X.; Silbey, R.; Brédas; J.-L. *J. Am. Chem. Soc*. **1998**, *120*, 1289; Cornil, J.; Beljonne, D.; dos Santos, D. A.; Calbert, J. P.; Brédas, J.-L. *Thin Solid Films* **2000**, *363*, 72.

(26) Shi, Y.; Liu, J.; Yang, Y. *J. Appl. Phys.* **2000**, *87*, 4254.

(27) Nguyen, T.-Q.; Yee, R. Y.; Schwartz, B. J. *J. Photochem. Photobio.*, in press; Zheng, Y.; Min, Y.; MacDiarmid, A. G.; Angelopolous, M.; Liao, Y.-H.; Epstein, A. J. *Synth. Met.* **1997**, *84*, 109.

(28) Hong, J.-D.; Kim, D.; Cha, K.; Jin, J. *Synth. Met.* **1997**, *84*, 815.

(29) Teetsov, J.; Vanden Bout, D. A. *J. Phys. Chem. B.* **2000**, *104*, 9378.

(30) "Good" solvents are defined as solvents in which the polymer can dissolve completely after only a short period of time (several hours), while "poor" solvents are those in which a much longer period of time is required for the polymer to dissolve (≥ a day).

(31) Schaller, R. D.; Lee, L. F.; Johnson, J. C.; Haber, L. H.; Saykally, R. J.; Nguyen, T.-Q.; Schwartz, B. J. *Phys. Rev. Lett.*, submitted.

(32) Papadimitrakopoulos, F.; Konstandinidis, K.; Miller, T. M.; Opila, R.; Chandross, E. A.; Galvin, M. E. *Chem. Mater.* **1994**, *6*, 1563; Papadimitrakopoulos, F.; Yan, M.; Rothberg, L. J.; Katz, H. E.; Chandross, E. A.; Galvin, M. E. *Mol. Cryst. Liq. Cryst.* **1994**, *256*, 663.

(33) Yan, M.; Rothberg, L. J.; Papadimitrakopoulos, F.; Galvin, M. E.; Miller, T. M. *Phys. Rev. Lett.* **1994**, *73*, 744.

(34) See, e.g., Higgins, D. A.; Barbara, P. F. *J. Phys. Chem.* **1995**, *99*, 3; Vanden Bout, D. A.; Kerimo, J.; Higgins, D. A.; Barbara, P. F. *J. Phys. Chem.* **1996**, *100*, 11843; Weston, K. D.; Carson, P. J.; Metiu, H.; Buratto, S. K. *J. Chem. Phys.* **1998**, *109*, 7474; McNeill, J. D.; O'Connor, D. B.; Barbara, P. F. *J. Chem. Phys.* **2000**, *112*, 7811; Dunn, R. C.; Holtom, G. H.; Mets, L.; Xie, X. S. *J. Phys. Chem.* **1994**, *98*, 3094; Betzig, E.; Chichester, R. J.; Lanni, F.; Taylor, D. L. *Bioimaging* **1993**, *1*, 129; Ennderle, Th.; Ha, T.; Chemla, D. S.; Weiss, S. *Ultramicroscopy* **1998**, *71*, 303.

(35) DeAro, J. A.; Weston, K. D.; Buratto, S. K.; Lemmer, U. *Chem. Phys. Lett.* **1997**, *277*, 532.

(36) Schaller, R. D.; Roth, C.; Raulet, D. H.; Saykally, R. J. *J. Phys. Chem B* **2000**, *104*, 5217; Schaller, R. D.; Johnson, J. D.; Saykally, R. J. *Anal. Chem.* **2000**, *72* 5361.

(37) Wudl, F.; Alleman, P. M.; Srdanov, G.; Ni, Z.; McBranch, D. *ACS Symp. Ser.* **1991**, 455.

(38) Hoffman, P.; Dutoit, B.; Salathe, R.-P. *Ultramicroscopy* **1995**, *61*, 165.

(39) Webster, S.; Smith, D. A.; Batchelder, D. N.; Lidzey, D. G.; Bradley, D. D. C. *Ultramicroscopy* **1998**, *71*, 275; Hsu, J. H.; Wei, P. K.; Fann, W. S.; Chuang, K. R.; Chen, S. A. *Ultramicroscopy* **1998**, *71*, 263; Stevenson, R.; Granstrom, M.; Richards, D. *Appl. Phys. Lett.* **1999**, *75*, 1574.

(40) This observation of the change in vibronic coupling to produce a relative increase of the 0-1 vibronic feature of the PL is also consistent with studies of the emission from PPV-based conjugated polymers under pressure. See, e.g, Webster, S.; Batchelder, D. N. *Polymer* **1996**, *37*, 4961; Tikhoplav, R. K.; Hess, B. C. *Synth. Met.* **1999**, *101*, 236.

(41) Klimov, V. I.; McBranch, D. W.; Barashkov, N. N.; Ferraris, J. P. *Chem. Phys. Lett.* **1997**, *277*, 109.

(42) Atriya, M.; Li, S.; Kang, E. T.; Neoh, K. G.; Ma, Z. H.; Tan, K. L.; Huang, W. *Polym. Degrad. Stabl.* **1999**, *65*, 287.

(43) Denton, G. J.; Tessler, N.; Harrison, N. T.; Friend, R. H. *Phys. Rev. Lett.* **1997**, *78*, 733.

(44) DeAro, J. A.; Gupta, R.; Heeger, A. J.; Buratto, S. K. *Synth. Met.* **1999**, *102*, 865. Credo, G. M.; Lowman, G. M.; DeAro, J. A.; Carson, P. J.; Winn, D. L.; Buratto, S. K. *J. Chem. Phys.* **2000**, *112*, 7864−72.

(45) See, e.g., Kersting, R.; Lemmer, U.; Mahrt, R. F.; Leo, K.; Kurz, H.; Bassler, H.; Gobel, E. O. *Phys. Rev. Lett.* **1993**, *70*, 3820; Ch. Warmuth, A. Tortschanoff, K. Brunner, B. Mollay, H. F. Kauffmann, *J. Lumin.* **1998**, *76&77*, 498; A. Watanabe, T. Kodaira, O. Ito, *Chem. Phys. Lett.* **1997**, *273*, 227.

(46) Wu, J.; Gross, A. F.; Tolbert; S. H. *J. Phys. Chem. B.* **1999**, *103*, 2374.

(47) Nguyen, T.-Q.; Wu, J.; Doan, V.; Schwartz, B. J.; Tolbert, S. H. *Science* **2000**, *288*, 652; Schwartz, B. J.; Nguyen, T.-Q.; Wu, J.; Tolbert, S. H. *Synth. Met.* **2001**, *116*, 35.

(48) Hu, D.; Yu, J.; Barbara, P. F. *J. Am. Chem. Soc.* **1999**, *121*, 6936−37; Vanden Bout, D. A.; Yip, W.-T.; Hu, D.; Fu, D.-K.; Swager, T. M.; Barbara, P. F. *Science* **1997**, *277*, 1074−77; Yu, J.; Hu, D. H.; Barbara, P. F. *Science* **2000**, *289*, 1327.

(49) Huser, T.; Yan, M.; Rothberg, L. J. *Proc. Nat. Acad. Sci. U.S.A.* **2000**, *97*, 11187.

(50) See, e.g., Scott, J. C.; Kaufman, J. H.; Brock, P. J.; DiPietro, R.; Salem, J.; Goitia, J. A. *J. Appl. Phys.* **1996**, *79*, 2745; Cumpston, B. H.; Parker, I. D.; Jenson, K. F. *J. Appl. Phys.* **1997**, *81*, 3716; Zyung, T.; Kim, J. J. *Appl. Phys. Lett.* **1995**, *67*, 3420.

(51) Huser, T.; Yan, M. *Synth. Met.* **2001** *116*, 333.

(52) Lee, T. W.; Park, O. O. *Appl. Phys. Lett.* **2000** *77*, 3334; Lee, T. W.; Park, O. O. *Adv. Mater.* **2000** *12*, 801.